Metrol. Meas. Syst., Vol. 32 (2025) No. 3, pp. 1–16
DOI: 10.24425/mms.2025.154670

PAN POLSKA AKADEMIA NAUK

METROLOGY AND MEASUREMENT SYSTEMS
Index 330930, ISSN 0860-8229
www.metrology.wat.edu.pl

M&MS

DETECTING VEHICLE INTER-AXLE DISTANCE, INCLUDING SCENARIOS WITH A LIFTED AXLE, THROUGH THE APPLICATION OF A MULTI-FREQUENCY IMPEDANCE MEASUREMENT SYSTEM THAT UTILIZES INDUCTIVE LOOP SENSORS

Zbigniew Marszałek[1)], Artur Ryguła[2)], Andrzej Maczyński[2)], Krzysztof Duda[1)]

1) AGH University of Krakow, Department of Measurement and Electronics, Mickiewicz Avenue 30, 30-059 Krakow, Poland (✉ *antic@agh.edu.pl*)
2) University of Bielsko-Biala, Department of Transport, Willowa 2, 43-309 Bielsko-Biala, Poland

Abstract

Analysing traffic data collected under varying conditions requires the categorization of vehicle types. One significant issue is that most of the sensors used in vehicle classification systems cannot detect a lifted axle, which often leads to incorrect vehicle categorization. This article recommends utilizing a multi-frequency inductive loop (IL) impedance measurement (MFILIM) system for measuring vehicle inter-axle distances, also in the case of lifted axles. Two slim IL sensors and two wide IL sensors are utilized in the proposed MFILIM system. The vehicle speed and inter-axle distances are evaluated using the vehicle magnetic profile (VMP) waveforms, which are derived from the IL impedance measurements taken simultaneously at three carrier frequencies for a single IL sensor. The potential of the proposed method was validated through a laboratory testbed (LTB) equipped with IL sensor models and vehicle models constructed on a 1:50 scale. Additionally, validation was conducted under real traffic conditions using a road testbed installed adjacent to a commercial weigh-in-motion (WIM) system. The results obtained from several different test vehicles, which passed through the measuring stations multiple times during the experiment, were selected for analysis. The analysis indicated that the MFILIM system outperformed the commercial WIM station by yielding smaller errors in determining inter-axle distances. In addition, it successfully detected a lifted axle in all cases and accurately determined its distance from adjacent axles.

Keywords: multi-frequency impedance, vehicle magnetic profile, inductive loop, Weight-in-Motion (WIM) system, wheelbase, intelligent transportation system (ITS), inter-axle distance, lifted axle, speed measurement, vehicle classification.

1. Introduction

From the perspective of traffic management systems, one of the fundamental data is the category of vehicles. In Europe, the COST323 classification is used primarily [1], while in the United States, it is the FHWA [2]. In addition, other vehicle classifications can be adopted to address specific issues or measurement methods [3].

Article history: received February 07, 2025; revised April 28, 2025; accepted May 09, 2025; available online July 03, 2025.

Every vehicle classification is based on the measurement of characteristic parameters of passing vehicles. The specific parameters are primarily dependent on the measurement method chosen. In [4], an overview of the most widely used measurement methods is presented, dividing them into sensor-based and image-based. A comprehensive overview of vehicle classification methods can be found in [5]. In most classifications that involve multiple categories of vehicles, both the number of axles and the distances between them are considered. The distance between axles is crucial in *Weigh-In-Motion* (WIM) systems. Depending on this distance, the adjacent axles will be classified as single or multiple axles, directly affecting their maximum permitted load. The distance between axes is also one of the key parameters in many systems that are used to guarantee the safety of bridges [6–8]. An additional challenge in the classification of heavy vehicles is the detection of a lifted axle. The axles can be lifted automatically or at the driver's discretion [9]. Failure to detect a lifted axle will result in incorrect classification. A Category 3 truck according to COST323 [1] will be classified as Category 2, while a Category 5 semi-truck will be classified as Category 4.

Although various sensors are used for vehicle classification, *inductive loops* (IL) dominate in Europe. The IL sensors function on the basis of the principle that a metallic object, such as a vehicle, disrupts the electromagnetic field generated by the induction loop embedded in the roadway. When a vehicle passes over or stops above the IL sensor, phenomena such as eddy currents, electromagnetic coupling, and ferromagnetic interactions within the vehicle's structure result in measurable changes in the impedance of the sensor [10–17]. Compared to other types of sensors, IL sensors are relatively inexpensive and durable [10, 11]. Initially, IL sensors were only used to detect the presence of a vehicle in the traffic lane and to measure its speed [12]. However, a set of IL sensors can provide much more data by analyzing the *vehicle magnetic profile* (VMP), such as the number of axles [10] and the distance between them [13], the total length of the vehicle [14, 15], the length of overhangs or even the suspension height [16]. IL sensors that utilize the multi-frequency impedance measurement method provide both *resistance* (R-VMP) and *reactance* (X-VMP) components of the VMP [17–21]. Simultaneous measurement of impedance at multiple frequencies improves immunity to *electromagnetic interference* (EMI) [13, 22].

Most VMP-based vehicle classification systems use typical IL sensors that are 1 to 2 m long [23]. In contrast, the proposed system consists of two wide IL sensors (1 m by 2 m) and two slim ones (0.1 m by 3.2 m), arranged alternately one behind the other at intervals of 0.2 m. Each IL sensor utilizes three different measurement frequencies; thus, it generates three R-VMP and three X-VMP signals [20].

The research presented in this paper was conducted in both the field, in real traffic conditions, and in the laboratory. In the field, the system was installed on a national road in Poland, adjacent to an operational Class B+(7) WIM station [1], which allowed for additional comparative analysis. In the laboratory, the tests were carried out on a test station purpose-built on a scale of 1:50 in a fully controlled environment, allowing the assessment of the theoretical potential of the method to determine both the speed of the vehicle and distance between its axles. The conducted research demonstrated that supplementing the WIM system sensors with slim IL sensors, along with the proposed *multi-frequency inductive loop impedance measurement* (MFILIM) system, is an effective solution for addressing the issue of detecting lifted axles in WIM systems. This approach also enables an accurate measurement of the distance between axles, providing a reliable input for vehicle classification. With the implementation of MFILIM, misclassifications are prevented for vehicles operating with a lifted axle.

The paper is organized as follows: Section 2 outlines the materials and methods, Section 3 presents the results, Section 4 contains the discussion, and Section 5 concludes with a summary of the findings.

Metrol. Meas. Syst., Vol. 32 (2025), No. 3, pp. 1–16
DOI: 10.24425/mms.2025.154670

2. Materials and methods

2.1. Roadside measurement systems

The roadside testing station is located on the national road DK44 in the city of Mikołów (50°13′05.8″N 18°49′56.6″E). On the specified road segment, the permissible speed for passenger vehicles is 70 km/h, while for heavy vehicles it is 50 km/h. The average daily traffic volume ranges around 8,000 vehicles per day, with heavy vehicles accounting for 12% of this volume. The layout of the MFILIM and WIM system is presented in Fig. 1. As part of the MFILIM measurement station, four IL sensors were installed in the road: two wide IL sensors measuring 1 m by 2 m (IL1 and IL3), and two slim IL sensors measuring 0.1 m by 3.2 m (IL2 and IL4), where the first dimension in each case corresponds to the direction of vehicle flow. The difference in lateral dimensions between the wide (2 m) and slim (3.2 m) sensors results from the varying ranges of their electromagnetic fields. Specifically, the wide sensors (IL1 and IL3) have a larger detection area and are primarily used for vehicle detection and speed measurement, whereas the slim sensors (IL2 and IL4) have a smaller detection area, focus on axle (wheels) detection and therefore they must cover the entire width of the lane.

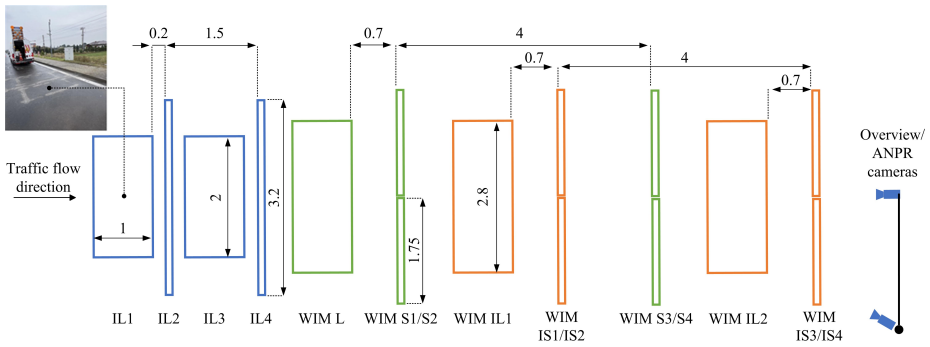

Fig. 1. Layout of the proposed MFILIM (blue), Intercomp commercial WIM system (green), and R&D WIM system (orange). Dimensions are shown in meters.

Importantly, two WIM stations operate on the respective road segment. One is a commercial station consisting of an IL sensor (WIM L) and four strain gauge load cell sensors (WIM S1-S4). The other WIM station, part of an R&D project, includes two IL (WIM IL1 and WIM IL2) and four strain gauge load cell sensors (WIM IS1-IS4). Each IL sensor in the WIM station measures 1 m by 2.8 m, while the strain gauge load cell sensors, manufactured by Intercomp [24], have a length of 1.75 m.

Commercial WIM stations achieve a measurement accuracy of B+(7) as defined by the COST323 specification [1]. According to this class, the confidence interval for the inter-axle distance is ±3%.

In May 2023, the commercial WIM station underwent a calibration procedure in accordance with the requirements set by the road administrator. During the calibration process, three types of heavy vehicles were used: a 2-axle truck, a 3-axle truck, and a 2-axle tractor with a 3-axle semi-trailer. Each vehicle passed over the WIM station 10 times as part of the verification runs. The measurement error for the inter-axle distance is presented in Fig. 2. The smallest error variation was achieved for the 2-axle truck, with measurement error not exceeding 1%. In contrast, for axle spacing measurements of the 2-axle and 3-axle vehicles, the error was significantly larger, although it remained within the range of ±3%.

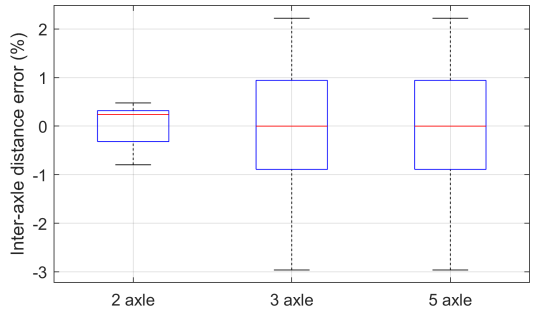

Fig. 2. Inter-axle distance error of the commercial WIM station while being calibrated in May 2023. The median is represented by a red line, while the 25th and 75th percentiles are indicated by blue lines at the bottom and top of a box, respectively. The highest and lowest data points are shown by black whiskers.

2.2. Multi-frequency inductive loop impedance measurement (MFILIM) system

Figure 3 depicts the proposed MFILIM system, which operates with four IL sensors that provide input signals to the *auto balancing bridge* (ABB), serving as the analog front end for the digital section of the system [22]. The measuring current is generated using 4 *digital-to-analog converters* (DAC), which supply input signals to the ABBs. The output voltages of the ABBs are measured by 8 *analog-to-digital converters* (ADCs). The MFILIM system is implemented on a PXI platform and operates synchronously.

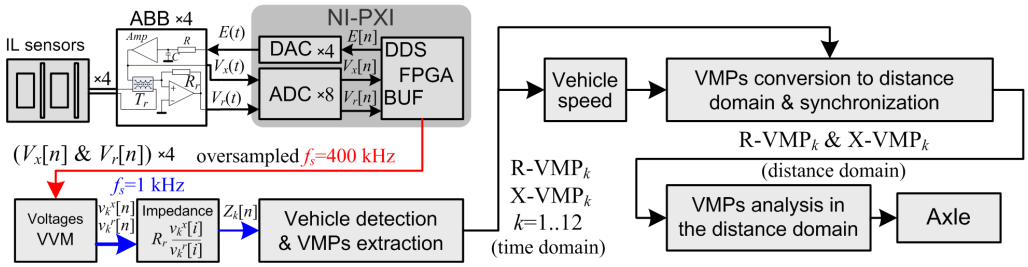

Fig. 3. Block diagram of the MFILIM system, where DAC – digital to analog converter, ADC – analog to digital converter, ABB – auto balancing bridge, VVM – vector voltmeter, Rr – reference resistor, V_x and V_r – ABB output voltages, E – excitation voltage.

The software runs continuously on the FPGA (NI PXI-7853R series). A *direct digital synthesizer* (DDS) generates multi-frequency signals that excite the current in each IL sensor through the ABBs. The DDS works with the $f_s = 400$ kHz sampling frequency. An excitation signal for a single IL sensor has the form:

$$E_l[n] = \sum_{k=3l-2}^{K=3l} A_k \sin(\omega_k n + \varphi_k) \tag{1}$$

where $l = 1, \ldots, 4$ is the number of an IL sensor, $\omega_k = 2\pi F_k / f_s$ is the normalized pulsation in radians of the discrete-time signal, A_k is the amplitude, F_k is the frequency in Hz, φ_k is the phase angle in radians selected to achieve the minimum value of the crest factor [17], the lower index k refers to the k-th frequency component of the excitation signal, and n denotes the sample number.

The $E[n]$ signal is converted into voltage using a DAC and a low-pass RC filter in the analog part (ABB). The list of frequencies used in individual processing channels is listed in Table 1.

Table 1. Values of the measurement frequencies used in the MFILIM system.

Given physical channel	**Dedicated frequency channel k**	**Frequency F_k (kHz)**		
		low	*medium*	*high*
#1: for wide IL1 Sensor 1	1, 2, 3	10	18	27
#2: for wide IL3 Sensor 2	4, 5, 6	13	21	28
#3: for slim IL2 Sensor 1	7, 8, 9	6	15	22
#4: for slim IL4 Sensor 2	10, 11, 12	7	16	24

The complex-valued voltages at the output of the ABB are calculated using a *vector voltmeter* (VVM) [20], and the VMPs are calculated from the complex voltages measured in the proposed MFILIM system. The signal flow is explained in Fig. 3. Complex-value voltages $V_x[n]$ and $V_r[n]$, directly recorded by ADCs, are discrete-time versions of their continuous-time counterparts $V_x(t)$ and $V_r(t)$. The signals $V_x[n]$ and $V_r[n]$ are demodulated simultaneously for all excitation pulsations ω_k using the *flat-top bandpass Hilbert transformers* (FTBPHT) implemented as FIR filters [25].

The ADCs operate synchronously with the DDS. The VVM operates similarly to the multi-frequency lock-in amplifier [19]. The voltages $V_x[n]$ and $V_r[n]$ are intentionally oversampled with a 400 kHz sampling rate for better amplitude resolution and higher noise immunity. The outputs of the VVM are next downsampled to the 1 kHz sampling rate. The obtained 1 ms resolution of the time waveforms was verified to be sufficient from the point of view of locating the axle in the vehicle body.

The impedance measurements are taken simultaneously for all 12 excitation frequencies. For every excitation frequency, the VVM provides a complex value signal at a rate of 1 kS/s, and the impedance signals are calculated at the same rate. The MFILIM system operates on 12 frequencies (see Table 1) and outputs 12 impedance signals simultaneously, which corresponds to 3 measurements for each of the 4 sensors. The intentionally introduced measurement redundancy is designed to enable accurate measurement of vehicle speed and inter-axle distance even in the presence of EMI.

The reliability of the multi-frequency system is superior to that of the single-frequency system because, if the impedance signal at a given frequency is disturbed, the algorithm can detect this and rely on the undistorted signals. Importantly, the proposed method retains information regarding the real part of the IL sensor's impedance, which is uncommon in other existing IL-based systems. The hardware components used to build the MFILIM system are listed in [20].

2.3. Computation of the VMP

The change in the impedance signal, $\Delta Z_k[n] = Z_k[n] - Z_k^{\text{offset}}$, is continuously monitored. If the sum of the moduli of $\Delta Z_k[n]$ exceeds a predefined threshold of 1Ω, a vehicle is detected, and the measurement data are stored in a file along with some data collected before exceeding the threshold (pre-trigger) and after the threshold is lowered (post-trigger). The extraction of a VMP is a process that involves analysing changes in resistance and reactance parameters (ΔR_k and ΔX_k) caused by a moving vehicle. The R_k and X_k signals are adjusted by a constant offset equal to the nominal resistance and reactance, which is computed as a baseline level before the vehicle's presence, derived from the pre-trigger portion of the impedance signal. This offset is then subtracted from the R-VMP and X-VMP signals.

An example of time-domain signals recorded by road-installed sensors (see Fig. 1) for a 5-axle truck with its third axle lifted is shown in Fig. 4.

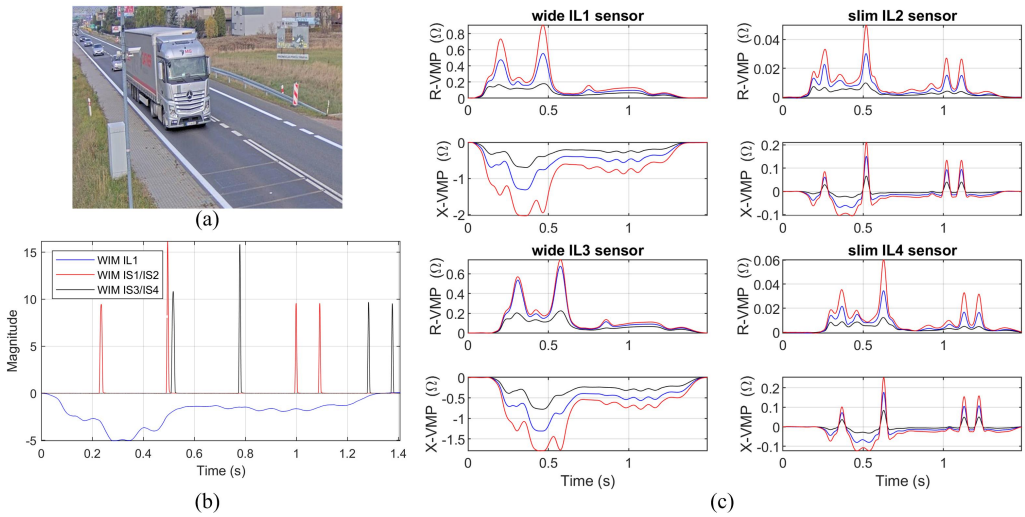

Fig. 4. Exemplary extracted data from the roadside measurement system: (a) vehicle photograph from the AMPR camera; (b) signals from the WIM system; (c) signals from the MFILIM system, where R- and X- denote resistance and reactance components VMP, respectively. The red, blue and black lines represent the VMPs for the highest, middle and lowest frequencies (Table 1), respectively.

2.4. Vehicle speed measurement

The vehicle speed is calculated based on the median time shift between the X-VMPs from the IL1 sensor and the X-VMPs from the IL3 sensor, which are mounted 1.5 meters apart. The use of X-VMPs is preferred because of their higher EMI immunity compared to that of R-VMPs. The time shift is determined by identifying the maximum value of the cross-correlation of the VMPs, following the normalization of each VMP by its absolute maximum value. Alternatively, the time shift can be calculated using the *discrete Fourier transform* (DFT) based algorithm, which provides fractional shift estimation and reduced computational complexity [26].

2.5. VMP representation in the distance domain

The known distance between sensors and the speed of the vehicle are used to represent the VMP as a function of the distance traveled by the vehicle rather than as a function of time, which is how it is typically measured. For this purpose, the adopted resolution for the distance axis is 1 cm. Subsequently, the respective VMPs from all IL sensors are adjusted by a distance equal to the appropriate mounting distances to the IL2 sensor (see Fig. 1). This process leads to VMP synchronization in the distance domain.

2.6. Axle detection using R-VMP and X-VMP of slim IL sensors

The representation of VMPs as a function of distance allows analysis of artifact positions caused by the axles of a passing vehicle, thereby allowing the determination of the distances between them. As shown in Fig. 4c, using slim sensors (IL2 and IL4), six R-VMP and six X-VMP

are obtained. In the distance domain, the signals from the IL4 sensor are synchronized with the signals from the IL2 sensor. Axle detection is performed using Algorithm 1, which extracts and enhances axle information from VMPs obtained via the slim IL sensors. First, the mean signals *R_VMP_mean* and *X_VMP_mean* are calculated by averaging the six normalized signals. The algorithm then identifies the minimum value in the *X_VMP_mean* vector and assigns its index to the variable k, while the corresponding value from *R_VMP_mean* is assigned to r. A gain factor is calculated as the ratio of the absolute value of x to r. The next step involves calculating the vector K, which is a linear combination of the *R_VMP_mean* and *X_VMP_mean*, scaled by the *gain* factor. This vector is then normalized to obtain the *AxleEn* signal, which represents the spiking axle signal.

Algorithm 1. Extracting the axle signal using VMPs from slim IL sensors.

Input: *R_VMP_mean* = *mean*(normalized_slim_IL_R_VMP)
Input: *X_VMP_mean* = *mean*(normalized_slim_IL_X_VMP)
$[x, k] = \min(X\_VMP\_mean)$
$r = R\_VMP\_mean(k)$
$gain = abs(x)/r$
$K = gain \cdot R\_VMP\_mean + X\_VMP\_mean$
$AxleEn = K/\max(K)$
$Comp = comparator(AxleEn)$
$Axle = mute(AxleEn, Comp)$
Output: *Axle*

The signal is passed through a comparator, which provides logical output. Finally, the output is used to mute the *AxleEn* signal, resulting in the final axle signal, *Axle*, which is the output of the algorithm. The detection of vehicle axles in the enhanced *AxleEn* signal is implemented by means of a software comparator with an adjusted comparison level. The *Comp* signal allows us to mute artifacts from chassis components other than axles. The sample indices of the maximum values found in the *Axle* signal are used in consecutive order to calculate the distance between the axles. Exemplary signals converted to the distance domain are presented in Fig. 5, along with the extracted axle signal and the detected axle locations [27]. The negative distances are the result of the reference system where the origin is set at the center of the sensor and aligned with the center of the vehicle's side silhouette. The third axle of the truck, which is lifted and does not exert any contact force on the WIM S1/S2 sensors, is successfully detected using slim IL sensors.

2.7. Laboratory testbed (LTB)

A dedicated *laboratory test-bed* (LTB) was constructed to evaluate the potential of the MFILIM method [27]. A conceptual diagram, including its components, is shown in Fig. 6a. During testing, the vehicle model moves at a certain speed around a circle with a fixed radius. During each lap, it passes through an IL sensor area. The IL sensor area comprises a set of four IL sensors arranged as illustrated in Fig. 6b. The unique design of the vehicle model (Fig. 6c) also facilitates EMI generation during the simulated operation of the vehicle's engine. The vehicle model and the IL sensors are constructed at a scale of 1:50.

The laboratory testbed consists of a motor, a planetary gearset, an encoder, and a programmable controller. The rotational velocity is regulated based on the encoder signal. The arm can be rotated at a specified rotational velocity for a predetermined number of laps. The EMI coil in the vehicle model is powered by a rotary connector mounted on the motor axle. The parameters of the drive

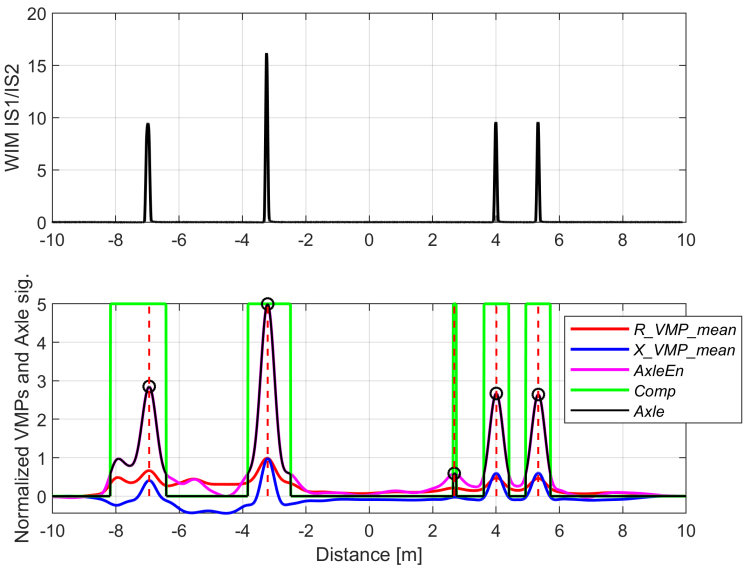

Fig. 5. Exemplary signals in the distance domain, top: WIM IS1/IS2 signal, bottom: normalized mean slim IL sensor *R_VMP_mean* and *X_VMP_mean*, and extracted *Axle* signal [27], and peak location detected (see Algorithm 1).

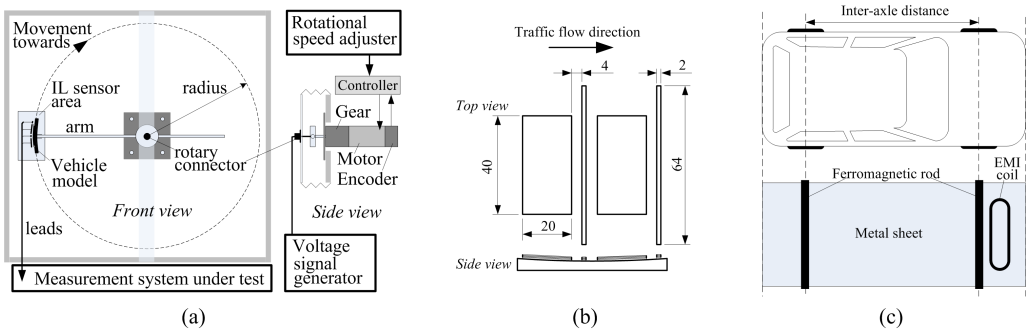

Fig. 6. Laboratory testbed: (a) schematic diagram, (b) model of IL sensors (dimensions in mm), (c) top-view of a vehicle silhouette for analysis and the two-axle physical vehicle model.

system are specified in [27]. This design of the drive system allows us to precisely control the rotational speed and, consequently, the speed component of the vehicle model, which is tangential to the lane of the vehicle's motion. The uncertainty in determining the tangential speed is 0.5% within the speed range, which corresponds to its real-world counterpart, from 10 km/h to 120 km/h.

2.8. Test Setup and Data Collection

In the LTB tests, the passenger vehicle model was investigated, while at the road testing station different types of vehicles were registered. Field measurements were carried out between 6-26 Nov 2024, resulting in a total of 140,000 recordings. For further analysis, vehicles of different categories were selected which repeatedly passed through the test station during the measurement

period. These were: a passenger car, a minibus, a city bus, a 3-axle truck, and a set – a tractor + a semi-trailer. The vehicles were identified on the basis of license plate numbers that are read by an Automatic Number Plate Recognition (ANPR) camera. The brands of the test vehicles were identified based on images from the overview camera, which allowed specific axle distance values to be retrieved from manufacturer catalog data. A list of the test vehicles, along with their inter-axle distances and the number of completed measurements, is summarized in Table 2. The adopted designations for the inter-axle distance of multi-axle vehicles, taking into account the possibility of lifting the third axle – the first axle of the semi-trailer, are shown in Fig. 7.

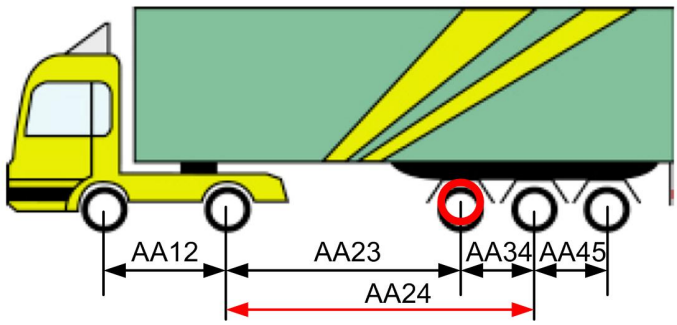

Fig. 7. Designations of the distance between the axles of a multi-axle vehicle including the lifted axle 3 [1].

Table 2. Test vehicles, nominal axle spacing, and number of measurements taken.

No	Vehicle	AA12 [cm]	AA23 [cm]	AA34 [cm]	AA45 [cm]	No of meas.
1	Laboratory model (LTB)	295	–	–	–	252
2	SUV (Skoda KODIAQ)	279	–	–	–	40
3	Bus 1 (BMC PROCITY)	585	–	–	–	115
4	Bus 2 (MAN TGE 5.180)	449.1	–	–	–	117
5	Truck 1 (MAN Faun Rotopress) – 3-axle	387.5	131	–	–	16
6	Truck 2 (Renault T HC 480 + semi-trailer) – 5-axle	360	600	131	131	10
7	Truck 2 (Renault T HC 480 + semi-trailer) – 4-axle (lifted axle no. 3)	360	AA24 = 731 cm		131	13

In further discussion, we refer to the relative percentage difference error, defined as:

$$E = \frac{x - r}{r} \cdot 100\,(\%) \tag{2}$$

where: x is the result of a single measurement and r is a reference (nominal) value.

The MFILIM system detects all axles of a vehicle and can indicate a lifted axle by analyzing the peak height in the *Axle* signal. In this case, the detection was additionally supported by a comparison of the results from the WIM IS1/IS2 sensors and the MFILIM system, along with a visual inspection based on the recorded image (Fig. 4a).

3. Results

3.1. LTB results

The tests carried out on the LTB served primarily to confirm the effectiveness of the MFILIM measurement method described in Section 2.2. A total of 252 model runs were conducted at various speeds ranging from 10 to 120 km/h. The speed of the vehicle and the distance between the axles were determined for each pass. Accurate measurement of speed is crucial for determining the axle distance accurately because it is the second component, apart from the distance between sensors, required to calculate the inter-axle distance. The box plot in Fig. 8a shows the variation of speed measurement errors, while the graph in Fig. 8b shows the variation of errors in detecting the distance between the axles.

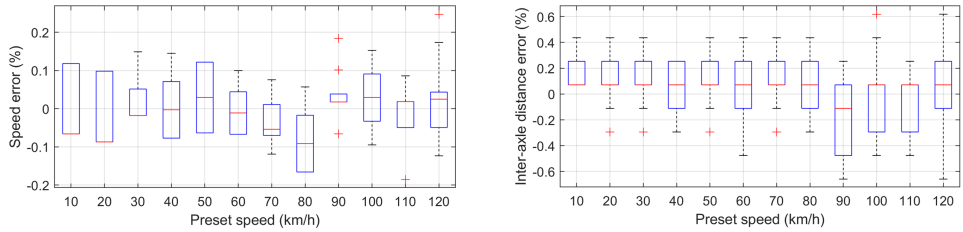

Fig. 8. Errors determined on the LTB for (a) speed and (b) inter-axle distance of the vehicle model. Red plus (+) markers denote outliers.

According to the requirements of COST323 [1], the error in determining the speed (above 30 km/h) and the vehicle inter-axle distance for the WIM Class A (5) stations must be within ±2%. The measurement errors obtained in laboratory tests on the LTB are significantly lower than these limits. Indeed, according to the graphs in Fig. 8a and 8b, they are within ±0.3% and ±0.7%, respectively, for the entire range of speeds analysed. For speeds up to 100 km/h, the error ranges are even noticeably smaller. This is important because measuring stations are usually placed on road sections with certain speed limits. In conclusion, the results obtained on LTB should be considered promising.

3.2. Road testing station results

Laboratory tests were performed under strictly controlled conditions. To assess the effectiveness of the proposed method in typical traffic scenarios, measurements were taken at the road testing station. As a first step, a validation of the speed measurement was performed by comparing the results obtained from the MFILIM measurement station and the WIM station. Fig. 9a shows the variation of the relative differences of the test vehicle speed measurements made by the two stations. A summary box plot of the variation of speed determination errors for all measurements obtained at the LTB is also added for comparison. The vehicle designations are consistent with those listed in Table 2, in which case the fact that the axle was lifted/lowered in Truck 2 is irrelevant.

The field measurements presented in Fig. 9a, in relation to the WIM station, are worse than those obtained under laboratory conditions. The speed measurement error of the WIM station is ±3%. Additionally, the speed is measured by both the MFILIM system and the WIM station at slightly different locations on the road, as illustrated in Fig. 1. Any potential changes in vehicle speed during measurement introduce further error. Nevertheless, the speed measurements obtained

Metrol. Meas. Syst., Vol. 32 (2025), No. 3, pp. 1–16
DOI: 10.24425/mms.2025.154670

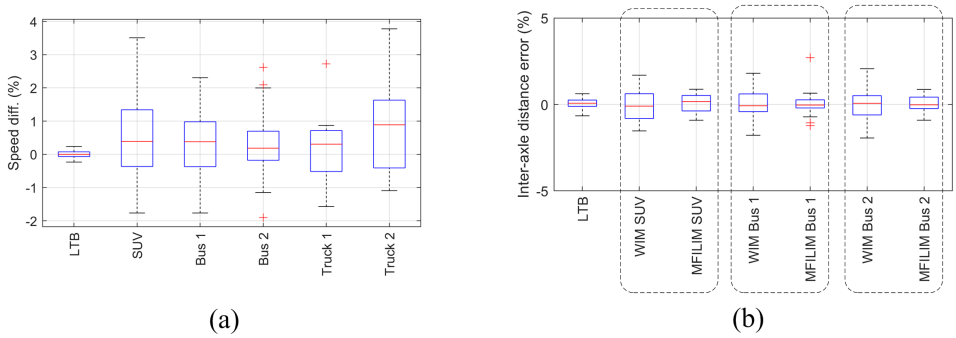

Fig. 9. (a) Relative percentage differences in speed measurements taken by the proposed MFILIM and reference WIM stations, and the summed box plot for the results obtained at the LTB, (b) Variability of inter-axle distance determination errors for 2-axle vehicles.

from the proposed MFILIM system and the commercial WIM station show good agreement, with the maximum relative percentage difference ranging from -2% to 4%. The results in Fig. 9 confirm the consistency of the proposed MFILIM system; however, determining its accuracy would require a high-accuracy method, such as road radar, which was not available at the time of the experiment.

For the error analysis of inter-axle distance determination, the measurement results obtained from both the MFILIM and the WIM systems were used. This approach allowed for a direct assessment of the quality of the MFILIM measurement compared to the commercial WIM system. The graphs in Fig. 9b show the variation of inter-axle distance determination errors for 2-axle vehicles. Two box plots were created for each vehicle: one representing the measurements taken by WIM and the other by MFILIM. In addition, a summary box plot was also added for all measurements obtained at the LTB.

The variation of the errors in determining the inter-axle distance by the two systems under consideration for a 3-axle vehicle is presented in a graph in Fig. 10a and for a 5-axle vehicle in a graph in Fig. 10b. In the latter case, the passes of the 5-axle vehicle with both lifted and lowered third axle are included. Since the WIM system does not detect a lifted axle, it only determines the AA24 distance for this vehicle configuration. The MFILIM system recorded the lifted axle in each case. Therefore, for comparison purposes, the distance AA24 for the MFILIM system was calculated as the sum of the distances AA23 and AA34.

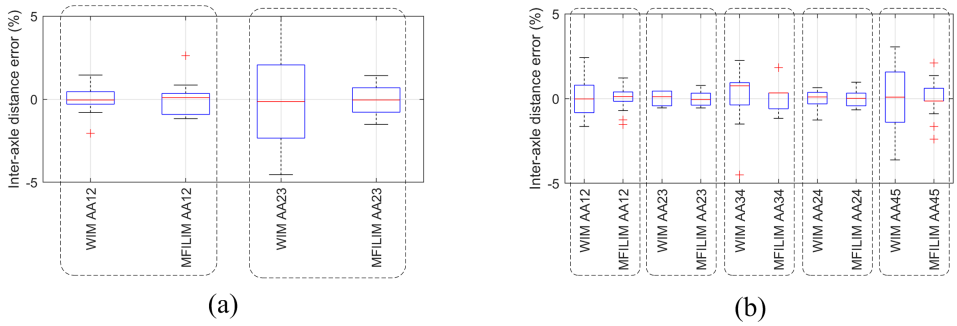

Fig. 10. (a) Inter-axle distance determination errors for a 3-axle vehicle. (b) Inter-axle distance determination errors for a 5-axle vehicle.

Table 3 provides basic descriptive statistics of inter-axle distance determination errors for both systems. The statistics include all measurements without distinguishing between vehicles and individual axles. Analysis of these data also indicates less variability in the error of the measurements obtained using MFILIM.

Table 3. Basic descriptive statistics for inter-axle distance determination errors.

	Average	**Median**	**Std**	**Minimum**	**Maximum**
WIM (%)	0	0	1.07	–4.54	5
MFILIM (%)	0	–0.02	0.57	–2.40	2.7

As expected, the variability of errors in determining the axle distance under traffic conditions is greater than under laboratory conditions. At the same time, analysis of the graphs in Fig. 9, 10 and Table 3 indicates that the proposed MFILIM system outperforms the commercial WIM system. For the most part, the errors for MFILIM are within ±2%, thus meeting the most stringent requirements for WIM class $A(5)$ stations [1].

4. Discussion

The laboratory and traffic tests of the MFILIM system presented in this paper have verified its potential for determining inter-axle distance, including lifted axles. The variability of the measurement errors, both in terms of vehicle speed and axle spacing, obtained on the LTB for a wide range of speeds, remains at a very low level, definitely less than ±1%. It can therefore be assumed that the method will also be useful in real traffic conditions.

In traffic conditions, many factors that interfere with the measurement must be considered. These include aspects such as the quality of the pavement around the testing station (unevenness, ruts, cracks), weather conditions (wind, precipitation, pavement condition) and the dynamics of vehicle passage (changes in speed and direction of passage, variation of forces in the vehicle's suspension, location of passage through the sensors). So, to confirm the conclusions of the laboratory tests, the MFILIM system was tested at a roadside testing station located right next to an existing WIM station. This approach allowed a direct comparison of the results obtained from MFILIM with the commercial WIM system which has been in operation for years.

In terms of speed measurement, validation was carried out by determining the variability of the difference in measurements taken by the MFILIM system and the WIM station. For all five vehicle categories tested, the differences were within ±4%. Given that the permissible speed measurement error for the WIM station is ±3%, this result should be considered fully satisfactory.

In this paper, the primary focus is on the potential application of the MFILIM system to measure the inter-axle distance of vehicles, including scenarios where one of the axles is lifted. Detecting a lifted axle and determining its distance from the other axles can be critical in categorizing vehicles. Identifying the brand names of the test vehicles, specific values for their axle distance were obtained from the catalog data. This, in turn, allowed for an analysis of error variability to be performed separately for the MFILIM system and the WIM system. As can be seen from the results presented in Section 3, the error variability for the proposed MFILIM system is not only lower than for the compared commercial WIM system, but it also meets the most stringent requirements of COST 323 [1]. It is very important that the lifted axles were detected in all cases. Additionally, it was not observed that the lifted axles significantly impacted the measurements of their distance from the adjacent axles.

In the final system, to enhance accuracy and increase the system's independence from variations in vehicle speed, the slim IL sensors should be positioned closer to the load-cell sensors. The space between the load-cell sensors can be used for this purpose.

5. Conclusions

The paper introduces the design fundamentals and application of the proposed MFILIM system. Laboratory and road testbeds equipped with the MFILIM system are investigated. The LTB test conducted over a wide range of speeds related to the measurement of driving speed and axle spacing yielded highly promising results. Under real traffic conditions, the validation of the MFILIM system for speed measurement was carried out by comparing the results with those obtained from a nearby WIM station. Validation was carried out for five vehicle categories. Subsequent analyses involved comparing the variability of inter-axle distance determination errors. The results indicate that the proposed MFILIM system has a higher accuracy than the commercial WIM system. What is particularly noteworthy is that the MFILIM system, unlike the WIM system, detects lifted axles and accurately calculates the distances between them and adjacent axles. The research and analysis carried out confirm the usefulness and significant potential of MFILIM-based systems in various road tests, including those related to vehicle categorization.

The MFILIM system not only improves vehicle classification efficiency by detecting a lifted axle but also allows independent measurement of the real part of the impedance. This capability is crucial for monitoring and identifying deteriorating or poor contact conditions in the IL sensor circuit. It is important to note that commonly used LC generator-based systems, even when operating under poor wire contact conditions, can still detect vehicles and generate a magnetic profile. However, these profiles may include additional artifacts that can adversely impact profile-based classification. The authors intend to continue work related to the development and implementation of MFILIM systems. In particular, new research opportunities will arise from the integration of MFILIM and WIM systems located in a single location [28–31].

Acknowledgements

The research project was partly supported by the program "Excellence initiative – research university" for the AGH University of Krakow.

References

[1] Jacob, B., O'Brien, E. J. & Jehaes, S. (Eds.). (2002). *COST 323. Weigh-in-Motion of road vehicles: Final report of the COST 323 action* (Vol. 1, p. 538). LCPC.

[2] Federal Highway Administration. (2013). *Traffic monitoring guide: Appendix C. Vehicle types*. U.S. Department of Transportation. https://www.fhwa.dot.gov/policyinformation/tmguide/tmg_2013/vehicle-types.cfm

[3] Zhao, H., Wu, D., Zeng, M. & Zhong, S. (2018). A Vibration-Based Vehicle Classification System using Distributed Optical Sensing Technology. *Transportation Research Record Journal of the Transportation Research Board*, 2672(43), 12–23. https://doi.org/10.1177/0361198118775840

[4] Tan, S. H., Chuah, J. H., Chow, C., Kanesan, J. & Leong, H. Y. (2023). Artificial intelligent systems for vehicle classification: A survey. *Engineering Applications of Artificial Intelligence*, 129, 107497. https://doi.org/10.1016/j.engappai.2023.107497

[5] Shokravi, H., Shokravi, H., Bakhary, N., Heidarrezaei, M., Koloor, S. S. R. & Petrů, M. (2020). A review on vehicle classification and potential use of Smart Vehicle-Assisted Techniques. *Sensors*, 20 (11), 3274. https://doi.org/10.3390/s20113274

[6] Lansdell, A., Song, W. & Dixon, B. (2017). Development and testing of a bridge weigh-in-motion method considering nonconstant vehicle speed. *Engineering Structures*, 152, 709–726. https://doi.org/10.1016/j.engstruct.2017.09.044

[7] Wu, Y., Deng, L. & He, W. (2020). BWIMNET: A novel method for identifying moving vehicles utilizing a modified encoder-decoder architecture. *Sensors*, 20 (24), 7170. https://doi.org/10.3390/s20247170

[8] He, W., Liu, J., Song, S. & Liu, P. (2023). A non-contact vehicle weighing approach based on bridge weigh-in-motion framework and computer vision techniques. *Measurement*, *225*, 113994. https://doi.org/10.1016/j.measurement.2023.113994

[9] Keleş, T., Güvenç, L. & Altuğ, E. (2019). ECU controlled intelligent lift axle dropping and lifting system for heavy trucks. *Engineering Science and Technology, an International Journal*, *22*(3), 885–893. https://doi.org/10.1016/j.jestch.2019.01.010

[10] Gajda, J., Piwowar, P., Sroka, R., Stencel, M. & Zeglen, T. (2011). Application of inductive loops as wheel detectors. *Transportation Research Part C: Emerging Technologies*, *21*(1), 57–66. https://doi.org/10.1016/j.trc.2011.08.010

[11] Mocholi-Salcedo, A., Arroyo-Nunez, J. H., Milian-Sanchez, V. M., Palomo-Anaya, M. J. & Arroyo-Nunez, A. (2016). Magnetic field generated by the loops used in traffic control systems. *IEEE Transactions on Intelligent Transportation Systems*, *18*(8), 2126–2136. https://doi.org/10.1109/tits.2016.2632972

[12] Ki, Y. & Baik, D. (2006). Model for accurate speed measurement using double-loop detectors. *IEEE Transactions on Vehicular Technology*, *55*(4), 1094–1101. https://doi.org/10.1109/tvt.2006.877462

[13] Marszalek, Z., Gawedzki, W. & Duda, K. (2020). A reliable moving vehicle axle-to-axle distance measurement system based on multi-frequency impedance measurement of a slim inductive-loop sensor. *Measurement*, *169*, 108525. https://doi.org/10.1016/j.measurement.2020.108525

[14] Belenguer, F. M., Salcedo, A. M., Ibañez, A. G. & Sánchez, V. M. (2019). Advantages offered by the double magnetic loops versus the conventional single ones. *PLoS ONE*, *14*(2), e0211626. https://doi.org/10.1371/journal.pone.0211626

[15] Coifman, B. & Kim, S. (2009). Speed estimation and length based vehicle classification from freeway single-loop detectors. *Transportation Research Part C: Emerging Technologies*, *17*(4), 349–364. https://doi.org/10.1016/j.trc.2009.01.004

[16] Marszalek, Z., Zeglen, T., Sroka, R. & Gajda, J. (2018). Inductive Loop Axle Detector based on Resistance and Reactance Vehicle Magnetic Profiles. *Sensors*, *18*(7), 2376. https://doi.org/10.3390/s18072376

[17] Yin, W., Dickinson, S. J. & Peyton, A. J. (2006). A multi-frequency impedance analysing instrument for eddy current testing. *Measurement Science and Technology*, *17*(2), 393–402. https://doi.org/10.1088/0957-0233/17/2/022

[18] Sanchez, B. & Bragos, R. (2010). Multifrequency simultaneous bioimpedance measurements using multitone burst signals for dynamic tissue characterization. *Journal of Physics Conference Series*, *224*, 012004. https://doi.org/10.1088/1742-6596/224/1/012004

[19] Sanchez, B., Fernandez, X., Reig, S. & Bragos, R. (2013). An FPGA-based frequency response analyzer for multisine and stepped sine measurements on stationary and time-varying impedance. *Measurement Science and Technology*, *25*(1), 015501. https://doi.org/10.1088/0957-0233/25/1/015501

[20] Marszalek, Z. & Duda, K. (2020). Multifrequency vector measurement system for reliable vehicle magnetic profile assessment. *Sensors*, *20*(17), 4933. https://doi.org/10.3390/s20174933

[21] Sui, J., Gandotra, N., Xie, P., Lin, Z., Scharfe, C. & Javanmard, M. (2021). Multi-frequency impedance sensing for detection and sizing of DNA fragments. *Scientific Reports*, *11*(1). https://doi.org/10.1038/s41598-021-85755-9

[22] Marszalek, Z., Konior, T., Izydorczyk, J., Szulik, M. & Duda, K. (2025). Vehicle classification based on Multi-Frequency Resistance and Reactance Magnetic Profiles. *IEEE Transactions on Intelligent Transportation Systems*, 1–10. https://doi.org/10.1109/tits.2025.3537137

[23] Chen-Fu, L. (2021). *Refining inductive loop signature technology for statewide vehicle classification counts* (Report No. MnDOT 2021-27). University of Minnesota, Department of Mechanical Engineering. https://mdl.mndot.gov/_flysystem/fedora/2023-01/202127.pdf

[24] Intercomp Company. (2017). *Weigh-in-motion strip sensor application guide*. https://www.intercompcompany.com/documents/Literature/700733-Strip-Sensor-APP-Guide.pdf

[25] Duda, K., Zielinski, T. P. & Barczentewicz, S. H. (2016). Perfectly Flat-Top and Equiripple Flat-Top Cosine Windows. *IEEE Transactions on Instrumentation and Measurement*, *65*(7), 1558–1567. https://doi.org/10.1109/tim.2016.2534398

[26] Duda, K. & Marszalek, Z. (2024). Vehicle speed determination with inductive-loop technology and fast and accurate fractional time delay estimation by DFT. *Metrology and Measurement Systems*, 781. https://doi.org/10.24425/mms.2024.152048

[27] Marszalek, Z. & Duda, K. (2024). Validation of Multi-Frequency Inductive-Loop measurement system for parameters of moving vehicle based on laboratory model. *Sensors*, *24*(22), 7244. https://doi.org/10.3390/s24227244

[28] Konior, A., Konior, T., Brzozowski, K., Maczyński, A. & Ryguła, A. (2023). New functionalities of the weigh-in-motion system: iWIM solution. *Transport Problems*, *18*(2), 161–170. https://doi.org/10.20858/tp.2023.18.2.14

[29] Burnos, P., Gajda, J. & Sroka, R. (2018). Accuracy criteria for evaluation of Weigh-in-Motion systems. *Metrology and Measurement Systems*, 743. https://doi.org/10.24425/mms.2018.124881

[30] Ryguła, A., Maczyński, A., Brzozowski, K., Grygierek, M. & Konior, A. (2021). Influence of trajectory and dynamics of vehicle motion on signal patterns in the WIM system. *Sensors*, *21*(23), 7895. https://doi.org/10.3390/s21237895

[31] Brzozowski, K., Maczyński, A., Ryguła, A., & Konior, T. (2023). A weigh-in-motion system with automatic data reliability estimation. *Measurement*, *221*, 113494. https://doi.org/10.1016/j.measurement.2023.113494

Zbigniew Marszałek received the M.Sc. degree in automatic and metrology and the Ph.D. degree in electrical engineering from the AGH University of Krakow, Poland, in 2008 and 2014, respectively. He is currently with the Department of Measurement and Electronics, AGH University of Krakow, where, since 2014, he has been assistant professor. His current research interests include Linux embedded systems, vehicle axle detection based on multi-frequency inductive-loop sensor technology, and vehicle in motion parameter measurement and classification systems.

Andrzej Maczyński, Ph.D., D.Sc., is an associate professor at the Faculty of Management and Transport at the University of Bielsko-Biala. For more than a dozen years he has served as the head of the Department of Transport. Initially, his research focused on the dynamics and control of mobile and offshore cranes. Currently, he is researching the application of Intelligent Transportation Systems to improve road safety and to assess and reduce the environmental impact caused by road traffic.

Artur Ryguła, received the M.Sc. degree in transport from the Silesian University of Technology, Poland, in 2007 and a Ph.D. degree in transport from the Kazimierz Pułaski Technical University of Radom, Poland, in 2012. Since 2014 he has been an assistant professor at the Faculty of Management and Transport of the University of Bielsko-Biala. He participates in the implementation and operation of ITS systems. His research interests include weigh-in-motion systems and traffic engineering.

Krzysztof Duda received the M.Sc. degree in automatics and metrology and the Ph.D. degree in electronics from the AGH University of Krakow, Poland, in 1998 and 2002, respectively. He has been with the Department of Measurement and Electronics, AGH University, where, from 2002 to 2019, he was an assistant professor and since 2019, he has been a professor. His current research interests include the development and applications of digital signal processing and analysis.